

Dear Editor,

The paper "Monitoring surface deformation of deep salt mining in Vauvert (France), combining InSAR and leveling data for multi-sources inversion" by Furst S, Doucet S, Vernant P, Champollion C, and Carme J-L, presents a study of the surface deformation above the salt mines in Vauvert, including a modeling part.

The paper and the approach are interesting but the paper suffers from many weaknesses in its current form. First, the writing has to be improved throughout the whole ms, and many English mistakes could have been avoided (I started to list all of them but I stopped, see below, I highlighted most of the small corrections in the pdf version). Second, I suggest to improve the structure of the paper, and particularly within each section, where many redundancies and confusions are spoiling the study. Third, the paper suffers from an unappropriated vocabulary, which is regrettable for a scientific paper. For instance, the word deformation is used over the whole text, whereas it should be displacement or velocity. Before publication, I would suggest the authors to add several major aspects on their study, according to the journal expectations. My suggestions/comments are listed below (in the order of the presentation of the paper); I am convinced that they will strengthen the paper, and help to emphasize the conclusions.

#### Introduction

The introduction should be rewritten. In its current form, it does not address clearly the problematics and the related methodological challenges. It is very hard to follow, since the structure is weak, with a section on the models, then on the data and data combination, then models again.

The authors forget to introduce the origin of the horizontal displacements. Are they induced by the slat flow? In this case, they should explain the process. Are they related to the centripetal displacements associated with the subsidence? This point is very important and should be better introduced in order to present the main objectives of the paper (L. 55-56)

Too many details regarding the models are given, whereas the main questions are not addressed yet. Therefore, it seems that more explanations are needed on important points (see L. 65-70, by the way this sentence should be with the following paragraph). Being in the introduction, some parts are lacking from clarity and important details (L. 50-52: this part is quite fast; the authors should be more clear about the models including a source with pressure or volume change (Mogi, penny-shape sill etc...))

#### Context and Data (section 2)

I would recommend to separate the context and the data.

Regarding the geological context, it is quite surprising that only one reference is cited.

Regarding the datasets, many questions and comments are rising. Surprisingly, it seems that the word technique and data are mixed several times. I would recommend to add a section on the accuracies of the measurements deduced from each technique, together with a discussion on the geometry of the displacements/velocity (LOS vs. vertical and horizontal). It is important to give the order of magnitude of expected surface H and V displacements/velocities and compare them with the accuracies of the geodetic techniques

used in this study. We wonder why the ALOS SAR images are not included in the study. Regarding the InSAR, the displacement data are the InSAR measurements and not the SAR images. Also, the authors use the word « develop a PS-InSAR processing chain » (L. 160), however I am quite sure that the chain has not been developed by them. Some sentences should be clarified (L. 169). The incidence angles and directions should be given in the data section and in the Figure 4. How are the InSAR-velocity uncertainties calculated?

The authors use the term « bowl » without clarify its cover on surface (see L. 195).

A major step is missing in the data/methodology for the InSAR data. How are the velocities calculated from InSAR displacements? Are the displacements stationary over time etc?

### Methodology

In the section 3.1, it should be more clear that the adjustment concerns the InSAR data to the other data. Some more details should be given regarding the horizontal shifts of the registration of the InSAR results, and how the manual detection is made (L. 212)? What do you mean by « reference system of InSAR data » (L. 213)? What are the quantitative arguments to consider that the PS density is sufficient to make the kriging?

The mathematical relations in the section 3.1.2 could be better written. The coordinate system should be clarified (N,E, Up or E,N,Up as in fig. 7?). How is the centre of the subsidence bowl chosen? What about the squint angle? The part related to the projection of the velocity along the profile is not clear.

The section 3.1.3 (kriging) is very unclear, whereas it is very important for the paper.

By refining the vertical velocities, it becomes possible for the authors to redefine the horizontal components of the velocities, or check that your initial assumptions are correct.

For the figure 7, I would recommend to plot the horizontal velocities with arrows and vertical with color.

Amplitudes reaching 20 mm/yr for the horizontal velocities are quite surprising, and are not consistent with the GNSS velocities. This kind of discussion should be included in the paper.

### Inversion

The authors claim « To infer the deep deformation using this combined dataset, the single dislocation plane is not sufficient to explain the horizontal motion. » (L. 302-303), but they should show it first. They should give more arguments, using the deep geometry of the mine. Looking at the results, it seems important to add a fourth row at depth. It is not serious in a scientific paper to just affirm in the discussion that it would not change the residuals. Less patches going deeper could be interesting. What about a simple Mogi source to explain subsidence and radial horizontal displacements?

L. 310: I have been lost. Why only 2 years, when you are using the whole dataset?

I remain doubtful regarding the inversion with 21 patches, and 63 free parameters to retrieve.

It should be mentioned that the depth is fixed. One more time, such a sentence « The optimal number of planes was found out by trial and error. », cannot be only mentioned, and not in the discussion part.

« The dislocations parameters are set free to vary between -1 and 1 m » : most of the parameters are angles?

The propagation of the uncertainties remains obscure.

What is the smoothing conditions between patches?

The series of tests of other models should not be in the discussion section (L. 443).

### Discussion

I suggest to make this part more structured (with subtitles for the several points to address).

The comparison of velocity amplitudes from the distinct datasets should mainly be in the result section, to validate or invalidate the approach.

What are the constraints within the mine for validate the model?

L. 453: how do you constrain the stress tensor from your model?

L. 455: I am pretty sure that stress measurements have been done in situ from many years.

I would remove the discussion with the Teil event, which seems out of the subject of the paper. We do know what is the purpose of the study! Reading at the discussion, we get the feeling that the problematics of the study is still unclear for the authors.

Acknowledgments:

The RESIF products should be references (DOI des données : 10.15778/resif.rg; <https://www.resif.fr/donnees-et-produits/donnees-gnss/>)

Figures:

Figure 1:

Caption of Figure 1: Change « concerned » by « area under study ». Is that a «Geological structural scheme » or a cross-section?

Figure 2:

What is the meaning of KemOne properties?

Caption of Figure 2: change techniques into data. Indicate the meaning of the purple areas.

Figure 3:

The axes need a title (distance along profile (km) vs. vertical displacement (mm)).

A color legend for the points is needed.

Caption of Figure 3: b) Time evolution of the vertical velocity of the marker... How is the velocity estimated?

Figure 4:

Specify that the covered area is the same than in Fig. 2b.

Figure 5:

Scale for velocity uncertainties are missing. The titles of the axes are « longitude (m) » and « latitude (m) ».

Figure 8: What is the decollement (detachment)? It should be mentioned in the text.

Caption: the purpose of the figure is only mentioned at the last sentence. Reverse the order

#### **Minor but important comments**

L. 22/23: « they » refers to what?

L. 22: change « desert » into « arid ».

L. 24: term « localized » requires quantification of dimensions of the areas.

L. 24: remove « for instance » if you use « such as »

L. 32: quantify « small »

L. 33: What do you mean by « and towards »?

L. 34+25: remove « s » to deformation.

L. 41: A previous study

L. 42: amplitude of surface velocity. Vertical? LOS? ...etc..

L. 44: Change « explore deformation at depth» into « estimate the surface deformation and infer the deformation at depth.

L. 45: be more precise about the typer of model

- L. 47: remove the « , » after although , and add an « s » to account, change « timewise » into « over time »
  - L. 48: change "surface deformation » into « surface data, such as displacements or velocities ».
  - L. 49: « On the other hand » requires first « On one hand ».
  - L. 50: deep source of strain
  - L. 51-55: From which observations?
  - L. 54: what about the depth? Is it fixed, using the knowledge of the caverns?
  - L. 57: degreeS, change « different » into « various »
  - L. 59: allows US to... (see L. 82, 185)
  - L. 60/61: what about the depth?
  - L. 61: What is the meaning of this sentence?
  - L. 62: associated WITH
  - L. 63: « deep deformation » or « deep sources »?
  - L. 64: « of » or « on »?
  - L. 65: meaning of « specifications »?
  - L. 71: « deformation velocities »: wrong term, change « different » into « distinct »
  - L. 74: references needed
  - L. 75: What do you mean by « ascending of parallel orbit »? Are your SAR images acquired from two distinct orbits?
  - L. 79: do you mean the space and time evolution of the deformation?
  - L.82: change « to estimate » into « the estimate of ».
  - L. 83: change « component of the deformation » into « components of the velocity field ».
  - L.83: remove « s » from « analyze »
  - L. 84: What is the meaning of « characterization »?
  - L. 87-89: Rephrase these sentences.
  - L. 90: What is the meaning of « global » here?
  - L. 91: Sentinel-1 (SAR images, not optic images from Sentinel-2 for instance), as well on L. 136.
  - L. 93: from InSAR data
  - L. 93: change « Then » by « In a second step »
  - L. 98: change « considering » into « taking into account ».
  - L. 103: reference needed.
  - L. 104: « distensive » is not correct, change « spreads » into « lasts », remove « -» (also L. 107)
  - L. 108: at depth
  - L. 110: not sure that « intercalations » is correct. Also, « insertion » L. 115.
  - L. 111: from
  - L. 117: Are those decimals reliable? Reference needed.
  - L. 123: « to more » is unclear?
  - L. 126: the other ones
  - L. 136: The SAR images are not geodetic data, InSAR data are!
  - L. 138: techniqueS
  - L. 144: precision, accuracy?
  - L. 145: measurements
  - L. 147-148: Rephrase.
  - L. 149: the profile, how many?
  - L. 151: associated WITH
  - L. 153: OF
- From now, I mainly underline the problems within the pdf version....
- L. 211: change LOS images into interferograms
  - L. 220: Define beta, because the flight directions are mentioned the beginning of the sentence, beta seems to be the look angle or LOS azimuth.
  - L. 235: what is the meaning of « process » here?
  - L. 245: Why this citation?
  - L. 260: not correct
  - L. 262-263: logical link not correct.
  - L. 253: should be given in the N, E, Up order
  - L. 296-7: should be in section 2.1 as well.
  - L. 313: plane direction? But you just mentioned the dip, so we expect the dip azimuth.
  - L. 315: do not produced
  - L. 335: do you mean assumptions?
  - L. 346: scenarii

L. 445: very confusing sentence

# Monitoring surface deformation of deep salt mining in Vauvert (France), combining InSAR and levelling data for multi-sources inversion

Furst S<sup>1</sup>, Doucet S<sup>2</sup>, Vernant P<sup>3</sup>, Champollion C<sup>3</sup>, and Carme J-L<sup>2</sup>

<sup>1</sup>Univ. Grenoble Alpes, Univ. Savoie Mont-Blanc, CNRS, IRD, IFSTTAR, ISTerre, 38000 Grenoble, France

<sup>2</sup>Fugro France, 115 Avenue de la Capelado, 34160 Castries, France

<sup>3</sup>Géosciences Montpellier, Université de Montpellier, CNRS UMR-5243, 34095 Montpellier, France

**Correspondence:** Séverine Furst (severine.furst@univ-smb.fr)

**Abstract.** The salt mining industrial exploitation located in Vauvert (France) has been injecting water at high pressure in wells to dissolve salt layers at depth. The extracted brine is used in chemical industry for more than thirty years, inducing a subsidence of the surface. Yearly levelling surveys monitor the deformation since the 1996. This dataset is supplemented by synthetic aperture radar images, and since 2015, GNSS data are also continuously measuring the deformation. New wells are regularly drilled to carry on with the exploitation of the salt layer, maintaining the subsidence. We make use of this careful monitoring by inverting the geodetic data to constrain a model of deformation. As InSAR and levelling are characterized by different strengths (spatial and temporal coverage for InSAR, accuracy for levelling) and weaknesses (various biases for InSAR, notably atmospheric, very limited spatial and temporal coverage for levelling), we choose to combine SAR images with levelling data, to produce a 3-D velocity field of the deformation. To do so, we develop a two-step methodology which consists first by estimating the 3-D velocity from images in ascending and descending acquisition of Sentinel 1 between 2015 and 2017, and second by applying a weighted regression kriging to improve the vertical component of the velocity in the areas where levelling data are available. GNSS data are used to control the resulting velocity field. We design an analytical model based on the geological and geophysical data. The model is made of 21 planes of dislocation with fixed position and geometry. We invert the combined geodetic dataset to estimate the slip and tensile motions of each plane. The results of the inversion highlight two behaviours of the salt layer: a major collapse of the salt layer beneath the extracting wells and a salt flow from the deepest and most external zones towards the centre of the exploitation.

**Keywords:** Geodesy; InSAR; Levelling; Monitoring subsidence; Data combination; Salt mining; Inversion; Reservoir modelling

*Copyright statement.* TEXT

## 20 1 Introduction

Rock salt (halite) is a sedimentary rock formed by the evaporation of sea water under specific conditions at different geological times. They are located underground or inside mountains, though some can also be found on the surface in desert regions. They mainly contain crystals of sodium chloride (NaCl), but can also include impurities such as clay, anhydrite or calcite. The distribution of salt deposits worldwide is very localized. In Europe, for instance, countries such as Germany, Denmark, and the Netherlands have a large amount of salt (Gillhaus and Horvath, 2008). The buried layers of rock salt can be dissolved by injecting water during the so-called solution mining process. This process is used to extract salt in the form of brine (for the chemical industry). More commonly, solution mining aims at creating salt caverns for the storage of fossil fuels such as natural gas, oil, and petroleum products (refined fuels, liquefied gas), but also for the storage of hydrogen and compressed air (Donadei and Schneider, 2016).

30 The difference in density between rock salt and the new material (brine, hydrocarbons) produces a change in stress equilibrium that leads to elastic and visco-elastic deformation of the surrounding medium (Bérest and Brouard, 2003; Bérest et al., 2006, 2012). This instantaneous (i.e. elastic) subsidence is relatively small for most salt and potash mines (Van Sambeek, 1993). Furthermore, a time-dependent subsidence also occurs, due to salt creeping into and towards production wells. This long-term subsidence continues until stresses have returned to their lithostatic values, reaching large deformations (1 m or more) over tens or hundred years (Van Sambeek, 1993). These dynamic surface deformations may result in damages to infrastructures (e.g. pipelines, roads, buildings, railways) in the vicinity of the exploitation. Therefore, to prevent these potential effects, long-term monitoring of the mining activities is usually mandated by governments. In this study, we focus on the particular monitoring of the deformation induced by rock salt mining in Vauvert (Southern France) using geodetic instruments and techniques. The extraction is performed by ones of the world deepest boreholes in salt reservoirs. The subsidence is monitored since 1996 using 1) levelling survey (IGN, Institut Géographique National), 2) SAR images acquired by various satellite missions (ERS, ENVISAT, SENTINEL) and 3) GNSS stations (both temporary and permanent stations). Previous study from Raucoules et al. (2003) has identified a subsidence bowl whose maximum amplitude reaches 22 mm/yr, by applying differential SAR Interferometry (DInSAR) technique to process ERS-1 and ERS-2 images from 1993 to 1999.

This long term and well documented monitoring provides exceptional datasets to explore deformation at depth. Indeed, a model of the salt layer can be derived in order to improve the brine productivity and to predict the evolution of subsidence. A software has already been developed for the Solution Mining Research Institute to evaluate and predict surface subsidence over underground openings (Van Sambeek, 1993). Although, this model account for three-dimensional geometry, the timewise distribution of the openings and salt creep, it does not include the surface deformation and considers caverns as voids in the salt layers (while brine remains in caverns at Vauvert's exploitation). On the other hand, geodetic data can be inverted to model deep strain sources in various systems such as for magmatic activities (e.g. Peltier et al. 2007; Camacho et al. 2011; Galgana et al. 2014), CO<sub>2</sub> injection (e.g. Vasco et al. 2008), stimulated reservoirs (e.g. Astakhov et al. 2012) or gas reservoir compartmentalization (e.g. Fokker et al. 2012). While the vertical component of the deformation observed in Vauvert can be reasonably modelled by a single point source, the horizontal component remains largely unexplained. Considering a 2-D plane

of dislocation to model the geometry of the salt layer (dimension, dip and azimuth) does not improve the fit to the horizontal components. One can postulate that with the salt extraction roughly in the center salt layer horizontal extension, the salt flow should induce horizontal displacements toward the well locations, hence a single plane cannot fit the observed deformation. Thus, by discretizing the salt layer into several planes of dislocation, we increase the degree of freedom for the sources to model the surface deformation. A series of inversions with different model configurations (number of sources, dimensions, orientations) allows to set the optimal number of dislocations for this study. We invert two years of recorded subsidence of the salt exploitation by modelling the deep salt layer as a collection of 21 planes of dislocation (Okada, 1992) with fixed position and geometry. We allow strike, dip slips and tensile dislocations for all planes to capture the relative movement of the salt layer. The inversion of geodetic data intends to retrieve these dislocation parameters (strike, dip, tensile) associated to each plane. The use of such complex model leads to a more complete interpretation of the deep deformation, including creep and loading (or not) of surrounding faults. However, it implies to deal with 3-D data. All three geodetic techniques measuring the subsidence in Vauvert are complementary regarding their spatial and temporal specifications. As a result, they can all be considered in the inversion process. But when it comes to the inversion of different types of data, one could combined the data before the inversion (e.g. Fuhrmann et al. 2015; Lu et al. 2015; Smittarello et al. 2019), jointly invert the data if all the different data are linked to a common physical model (e.g. Colombo et al. 2007; Geirsson et al. 2014; Palano et al. 2008; Segall et al. 2013) or assimilate new data at each time interval to improve the definition of the model (e.g. Bato et al. 2017; Hesse and Stadler 2014; Zhan and Gregg 2017). Because of the heterogeneous temporal and spatial coverage of geodetic data in Vauvert, we develop a methodology to combine deformation velocities from different geodetic datasets.

The combination of deformation data measured according to different geometries is not trivial. The displacement values are indeed projected along the line of sight of the satellite for InSAR, along the vertical for levelling and in 3D for GNSS. Different combination techniques have already been tested, at different stages of data processing. First, different satellite acquisition geometries (e.g. ascending, descending and ascending of parallel orbit) can be used to estimate the three components of the deformation (Wright et al., 2004). This implies that interferograms may cover slightly different time periods including information of the source at different time (Peltier et al., 2017). Second, combining data of different temporal and spatial sampling rates can be performed using methods of interpolation such as Gaussian process regression (kriging). These methods assume that the sampling is statistically representative (spatially and temporally) of the deformation area. For instance, Fuhrmann et al. (2015) developed a methodology to calculate and combine linear velocity rates from InSAR, levelling and GNSS data measured in the Upper Rhine Graben. InSAR, GNSS and levelling velocities are interpolated independently by ordinary kriging. Finally, these interpolated datasets are merged by a least squares adjustment allowing to estimate the North, East and Vertical component of the deformation. Similarly, Lu et al. (2015) analyzes levelling, PS and cross (between both datasets) variograms over the Choushui River Fluvial Plain in Taiwan. However, these methods are not suitable for the current study. Indeed, the interpolation methods (kriging and co-kriging) implicitly assume that the sample is statistically representative (spatially and temporally) of the deformation field. InSAR kriging works for most cases where the density of points allows the characterization of this deformation. But co-kriging, which uses two measurement techniques, assumes that this other technique (GPS,

levelling, tacheometry or inclinometry) is also statistically representative of the deformation (spatially and temporally). In the area of interest, levelling line and GNSS stations are located in well-defined areas.

90 In our study, we aim at characterizing the global deformation of salt reservoir using Sentinel images, levelling lines and GNSS data. We propose a two-step methodology to combine geodetic data measuring the bowl of subsidence induced by the salt extraction in Vauvert (Doucet, 2018). In the first step, we estimate the three components of the subsidence observed in Vauvert from Sentinel images. Then, we use regression-kriging technique in a second step, to constrain the vertical component of the deformation using levelling data. Considering the small number and the late installation of continuous operating GNSS  
95 stations (only partially matching the InSAR period), the resulting 3D velocities are not statistically representative in space and time. Therefore, they were not used to constrain the InSAR-based deformation field but only to control in first approximation the accuracy of the final deformation field. This latter is then inverted using a gradient-based method to characterize the dislocation parameters associated to the 21 planes of the model. Results are interpreted and discussed considering production data from the operator company, geological and geophysical complementary information.

## 100 2 Mining the deep rock salt deposit of Vauvert

### 2.1 Geological setting

The salt deposit of Vauvert is located on the NW margin of the on-shore half-graben of the extensional Camargue basin in southern France. This graben results from the Oligo-Aquitainian rifting of the margin during the Mediterranean Sea expansion. This distensive phase spreads from -30 to -15 My and affects the rim of the Alpine belt (Pyrenees, Languedoc, Gulf of Lion, Camargue, Valentinois, Bresse, Rhine plain). The NE-SW oriented basins are controlled by the SE-dipping Nîmes normal  
105 fault (Figure 1). Camargue basin contains up to 4000 m of syn-rift sediments which overlay a substratum of carbonates from Lower Cretaceous (+130 My). The rapid Oligo-Aquitainian sedimentation formed a succession of continental to lagunal series generally found between 900 and 4900 m deep (Figure 1, Valette and Benedicto 1995):

1. The Clay series gathers 2 sub-series: the "gray series" (2000 m-thick of deposit of clay, sand, limestone, marl, conglomerate and lignite) and the "red series" (200 m of clay and gypsiferous marls with several intercalations of marl and sand of palustrine environment);
2. The Saliferous series (900 m-thick) with four formations: the infra-saliferous, the lower saliferous, the intermediate marl and the upper saliferous formations;
3. The Marine clay series range from 800 to 1500 m-thick and correspond to three sequences of Aquitanian deposits, mainly  
115 composed of clay with insertion of limestones, sandstones or layers of dolomite.

During the Miocene crustal spreading, syn-rift sediments were covered by transgressive Burdigalian marine sediments and coastal molasses before being uplifted and eroded during the Messinian event (from 5.96 to 5.33 million years ago). The whole formation was finally overlaid by one last stage of sedimentation occurring during the Pliocene.

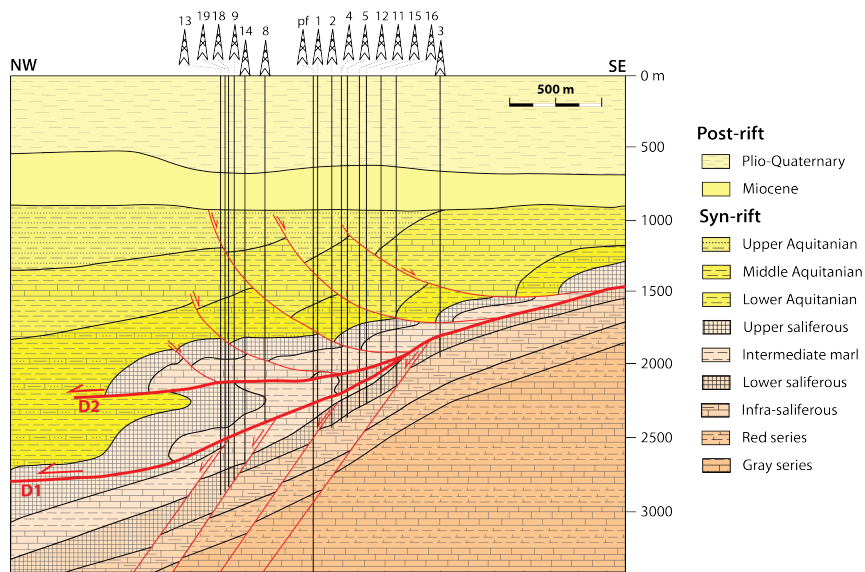


Figure 1. Geological structural scheme of the concerned area, Vauvert (from Valette and Benedicto 1995).

## 2.2 Salt extraction

120 The deep salt deposit of Vauvert has been discovered during the 1952-1962 oil survey conducted by ELF (Valette, 1991). Since 1972, the company KemOne (previously ELF ATOCHEM-Saline de Vauvert) is extracting the salt from deep reservoirs (1500-3000 m) in the form of a solution saturated in salt, the brine. The brine is then carried out to Fos-sur-Mer (70 km South-East of Vauvert) to be used in the chemical industry producing chlorine and caustic soda. The brine is recovered using two **to more** wells (doublets or triplets) hydraulically connected in the salt layer by initial or induced fracturing of the medium. Among

125 the current drilled wells (about 47), only **12** are still extracting brine, two are being drained (to release overpressure at well head due to salt creeping) and the **others** are abandoned. For the active sets, water is injected in one well at a pressure of 95 bars, while the second extracts the brine at 2 bars. The underground circulation of fluid is allowed by the induced fracturing created to connect the wells. Once the salt concentration in the brine reaches a minimum threshold (the extracted water does not contain enough salt to be exploited), doublets are abandoned and sealed. This implies an increase in pressure from bottom

130 to top of the wells, due to salt creeping. For security reason, the pressure needs to be released by opening the wells, allowing brine to flow and salt to creep until lithostatic equilibrium. In 2019, up to 1 million of tons of brine were extracted from about **4** active doublets (plus two as backup doublets).

## 2.3 Geodetic dataset

### 2.3.1 A wide network

135 The monitoring of salt extraction in Vauvert is performed since 1996 by IGN (Institut Géographique National) using levelling surveys (Figure 2a) along with a collection of SAR images acquired by various satellite missions (ERS, ENVISAT, SENTINEL). A permanent GNSS station was installed in November 2015 followed in October 2016 by three new permanent stations. Figure 2a represents the temporal coverage of all geodetic technique employed to monitor the site. In this study, we choose to derive an annual deformation velocity from InSAR analysis (Sentinel-1a/b images) images and levelling surveys  
140 measuring between 2015 to 2017, and permanent GPS data (2015-2019). Figure 2b shows the spatial coverage of levelling surveys and GPS networks used in this study.

### 2.3.2 Levelling surveys

The height differences between the different points of the network were determined by direct geodetic levelling (double run) carried out using an electronic level LEICA WILD NA3003, on a round trip pattern. This instrument has a resolution of 0.1 mm  
145 and the standard deviation of measurement for one kilometer of round-trip levelling is 0.4 mm (manufacturer data). IGN has conducted the processing using the Geolab least squares adjustment program (version 2001.9.20.0). This type of tool makes it possible to provide for each of the points an elevation as well as an indicator of the accuracy of the result in connection with the observations and not only from manufacturer nominal features. Figure 3 illustrates the levelling measurements performed between 1996 and 2018 along profile A-B on Figure 2b. These surveys started in 1996 with 39 levelling benchmarks, new ones  
150 were added progressively to densify the network and some needed to be replaced (destruction, shift, instability of a benchmark). Since 2006, about 130 benchmarks are measured yearly (except in 2013 and 2015). The deformation velocity associated to the subsidence is variable in time (Figure 3b), with a strong increase in the subsidence velocity between 2002 and 2003, since then the subsidence rate is relatively steady.

### 2.3.3 InSAR data

155 Radar images from Sentinel constellation imaging satellites (Sentinel-1a and Sentinel-1b) are recorded on the C-band frequency (similarly to Envisat) and present a short temporal redundancy of about 6 days, limiting the temporal decorrelations. The perpendicular baseline between the shots is very short, a few tens of meters, which also limits the spatial decorrelations. Sentinel constellation images have a swath of 250 km wide and a resolution of 5x20 m, in both ascending and descending geometries. In this study, we used respectively 101 and 66 images between April 18, 2015 to December 3, 2017 to produce a mean  
160 displacement velocity field and time series. To do so, we developed a PS-InSAR processing chain. The preparation of Single Look Complex (SLC) images and the creation of the interferograms are carried out with the software SNAP from the European Space Agency (ESA). Precise orbits provided by ESA (DORIS) are applied to finely process the geometric positioning of the image portions (bursts). Master image are chosen so that the time and the perpendicular baseline are optimized: images

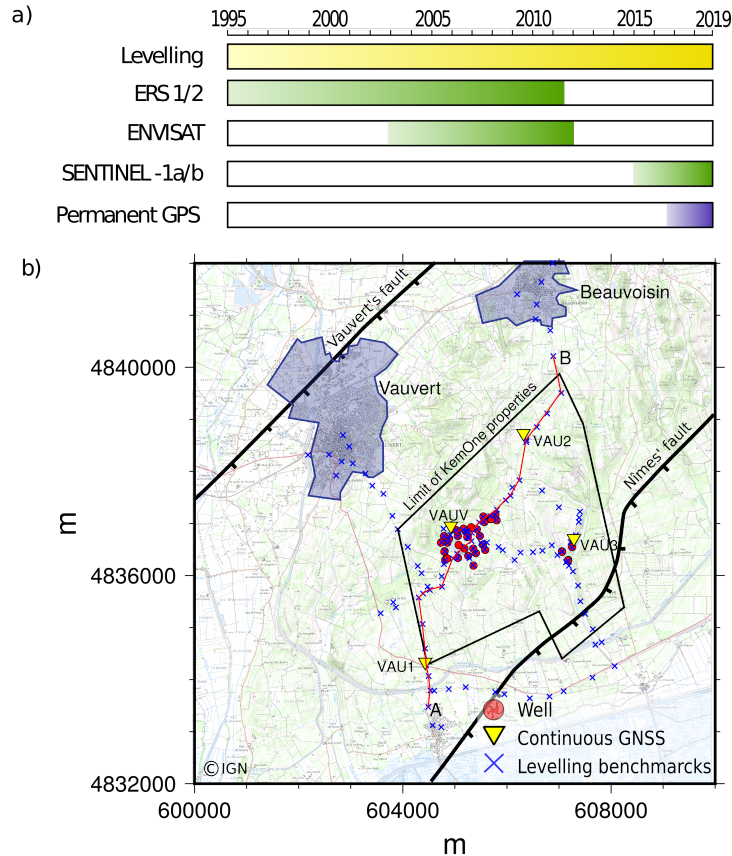


**Figure 2.** a) Temporal coverage of geodetic techniques available to monitor the site. b) Spatial coverage of GNSS and levelling network of the salt exploitation in Vauvert. Wellheads are represented by red circles, permanent GPS by yellow inverted triangles and levelling benchmarks are identified by blue crosses. The background map is extracted from IGN SCAN 1:25000 (©IGN).

of 26/11/2016 for the descending geometry and 27/11/2016 for the ascending geometry. The two SLC images (master image and slave image) of the same subdomain are co-registered using the orbits of the two products and the 90 m-resolution digital terrain model, SRTM (Farr and Kobrick, 2000; Farr et al., 2007). With known satellite orbits, a correction of the effect of the Earth's curvature on the phase is applied. The geodetic reference system is defined by the satellite orbit reference system (WGS84, the reference system used by all space SAR systems). The topographic phase is removed from the interferogram using the SRTM. Then the altitude information of each pixel is added to the product.

Once the interferograms are created under SNAP, they are imported and processed with StaMPS processing software (Hooper et al., 2004). The pixels are selected according to an amplitude dispersion criterion and a maximum proportion of "false" PS is

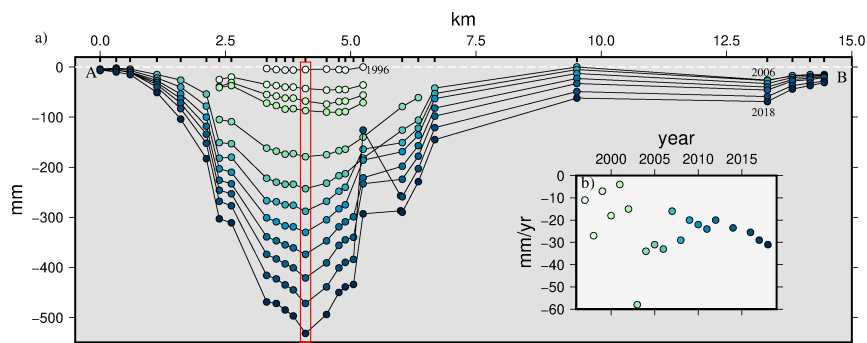


**Figure 3.** a) Levelling data along the A-B profile (red line on Figure 2b) performed by IGN from 1996 to 2018 (color scale). Data are displayed every two years for ease of reading. b) Deformation velocity associated to the marker with the largest subsidence (red rectangle in a). The velocity is given for each year, using the same color scale as in a).

set to 20%. DEM, Master atmosphere, orbit and look angle error are estimated, and removed. Finally, the fringes of the resulting phase are unwrapped (Figure 4a and b for ascending and descending geometries respectively). This allows to get position time-series which, using a linear regression, leads to velocities and associated uncertainties. The maximum subsidence rate is 24 mm/yr. The associated uncertainties are lower than 4.5 mm/yr for the ascending track and 2.9 mm/yr for the descending track with mean values of 1.2 mm/yr and 0.6 mm/yr respectively (Figure 4c and d).

### 2.3.4 Continuous GNSS

Four permanent GNSS stations (Figure 2) sampling at 30 s, were set up respectively in November 2015 (VAUV station) and October 2016 (VAU1, VAU2 and VAU3 stations) to characterize more accurately and in 3 dimensions the variations of the deformation and its spatial extension. The processing of coordinates and velocities is done using Gamit-Globk v10.7 software (Herring et al., 2015). We use the well-documented three-step approach and take advantage of the “realistic sigma” algorithm to estimate the uncertainties (see, Reilinger et al. 2006 for details). We include in the processing 26 continuous stable reference stations located within a 150 km radius of the Vauvert sites. These sites belong to the permanent RGP, RENAG (RESIF-RENAG French national Geodetic Network, RESIF – Réseau Sismologique et Géodésique Français) or ORPHEON networks and allow to define a stable regional reference frame by minimizing the velocities of these 26 sites. The resulting station position time series for the North, East and Vertical components are free of any regional tectonic displacement and show only local processes.

Figure 5a-c plots the time series of the three components of VAU3 station (Figure 2) from 2016 to 2019. Once the seasonal effects removed, the trends are quasi-linear in time for all three components. We represent the velocities of the sites near the exploitation with respect to a local stable reference frame on Figure 5d and e (i.e. all the velocities outside of the mapped area can be considered as equal to  $\sim 0$  mm/yr). The horizontal velocities (Figure 5d) measured at each station show a significant displacement toward the center of the exploitation. The vertical velocity (Figure 5e) indicates a maximum subsidence of -25.8

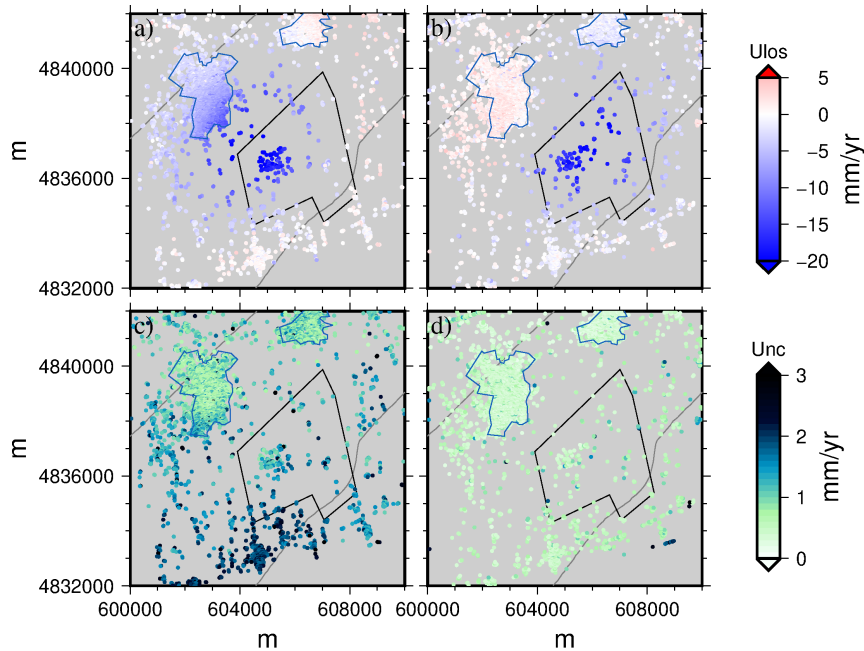


**Figure 4.** Mean velocity in LOS direction in a) ascending and b) descending interferograms over the area of interest (black polygon is KemOne properties boundary) and their associated uncertainties c) and d) respectively.

$\pm 0.2$  mm/yr but with greater magnitudes at the edges of the bowl ( $-13.8 \pm 0.7$  mm/yr at VAU3 and  $-17.9 \pm 0.7$  mm/yr at VAU2) than those previously measured (Raucoules et al., 2003). This may be due to a broadening of subsidence area during the period of measurements related to a temporary effect of well discharges or a potential increase in production.

### 3 Geodetic data combination

#### 3.1 Methodology

##### 3.1.1 General remarks on the combination

Terrestrial (e.g. levelling, inclinometry) or satellite-based (e.g. GNSS, InSAR) geodetic measurement networks are complementary to each other in terms of accuracy and spatial or temporal resolution, from slow ground displacement monitoring (e.g. Hastaoglu et al. 2017) to rapid surface changes (e.g. Peltier et al. 2017). Many attempts to combine these geodetic measurements have been described and published recently (e.g. Catalão et al. 2009; Burdack 2013; Lu et al. 2015), to overcome the limitations and inadequacies of the different techniques in difficult contexts, when taken separately (e.g. Karila et al. 2013; Abidin et al. 2015; Fuhrmann et al. 2015; Comerchi and Vittori 2019). The combination of several geodetic measurement techniques aims to improve the knowledge of the ground motion by overcoming or at least mitigating each technique shortcomings

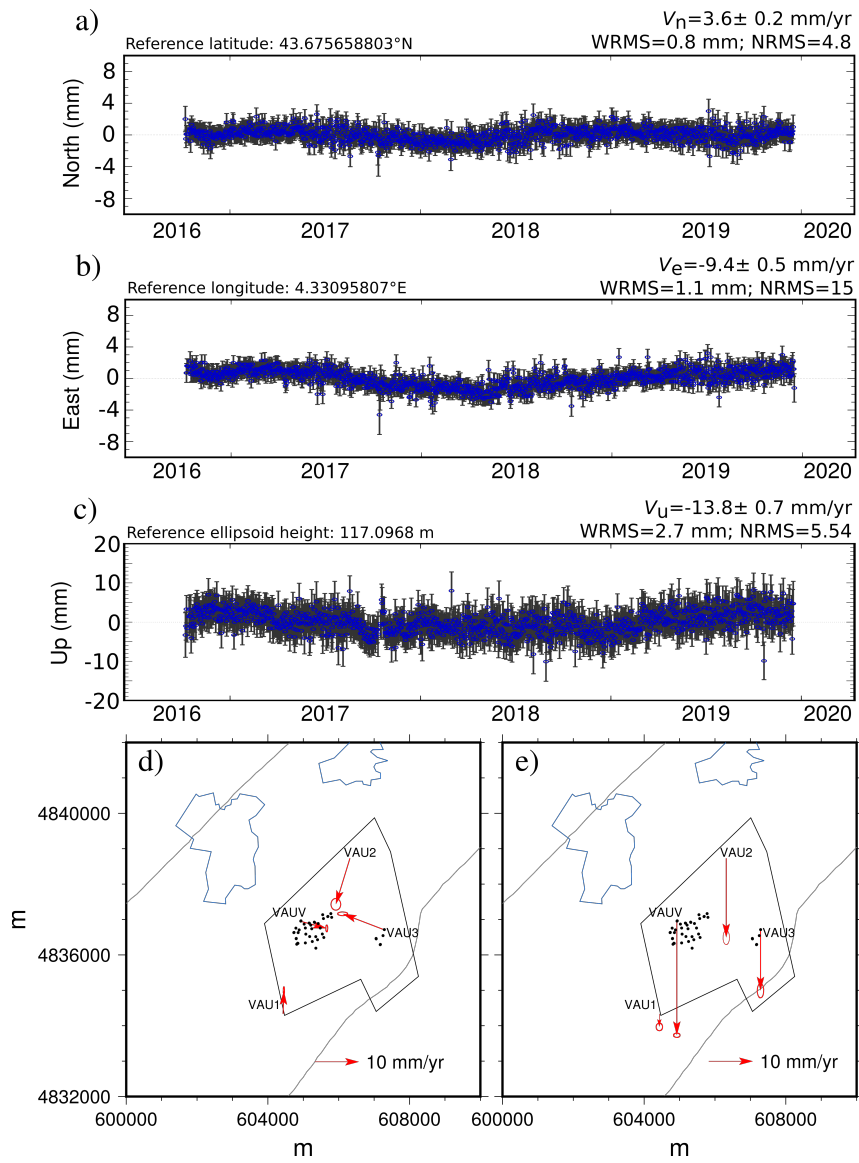


**Figure 5.** Time series of the three components a) North, b) East and c) Vertical, measured at station VAU3 from 2016 to the end of 2019. d) Map of horizontal velocities and well locations. e) Vertical velocities, downward being subsidence. Black polygon is KemOne properties boundary.

with the other. In this study, we propose a methodology to combine InSAR and levelling data to produce a 3D velocity field associated to the salt extraction of Vauvert (Doucet, 2018). The number of GNSS stations and, mostly the temporal coverage of time series are not statistically representative of the deformation for being appropriately incorporated in the combination (only

one out of four stations continuously measured the deformation between 2015 and 2017). Indeed the combination is based on  
210 the following assumptions :

1. **Reference frames adjustment.** In order to compare InSAR to levelling and GNSS data, we firstly correct the horizontal position of PS point using the mean value of all horizontal shifts manually detected on the LOS images. Secondly, we adjust the reference system of InSAR data using a two-dimensional linear ramp (Lundgren et al., 2009; Hammond et al., 2010) based on the calculation of differences between velocities at GNSS stations and PS data points near these stations.
- 215 2. **Sufficient measurement density.** We assume that the density of reliable permanent scatterers is sufficient for the considered area in both ascending and descending InSAR geometry results. Besides, we consider that levelling and InSAR measurements are dense enough to be statistically representative of the deformation. Hence their distribution can be interpolated using kriging methods (ordinary and weighted regression).
3. **Incidence look angles.** We assume that for the area of interest, flight directions of the satellite with respect to the North are symmetrical with respect to the North-South axis ( $\beta^{asc} = N103.96$  and  $\beta^{desc} = N256.01$  for all PS). The angles of incidence between the satellite and the permanent reflectors at the surface are considered near-identical in the ascending and descending geometry acquisition ( $\Theta^{asc} = 32.93^\circ$  and  $\Theta^{desc} = 36.98^\circ$ ). This allows us to estimate the East component of the deformation along with a near-vertical component.
- 220 4. **Radial deformation.** The surface deformation observed in the area of interest shows a quasi-symmetrical bowl of subsidence (Raucoules et al., 2003). We hence make the assumption that this symmetry affects all components of the deformation, leading to the estimation of the North component with an acceptable accuracy.
- 225

Although these hypotheses may be false for other cases, in the case of Vauvert, and given the previous available information from InSAR (Raucoules et al., 2003) and levelling, they allow to compute the first order three dimensional velocity field associated to the salt extraction. We review and comment these choices in the discussion regarding the results of both the combination and the inversion. Figure 6 represents the general algorithm of our two-step methodology to combine interferograms and levelling data involving 1) a 3D Geometrical estimation and 2) a weighted regression kriging.  
230

### 3.1.2 Step 1: 3D Geometrical estimation

The first step of the approach consists in interpolating the ascending and descending InSAR data by ordinary kriging, in order to densify the spatial distribution of PS points, so that they can be virtually colocated with levelling benchmarks. The kriging interpolation models the best linear unbiased prediction of the intermediate values by a Gaussian process (driven by prior covariances). The number of data points, position and uncertainties are considered in the interpolation, leading to interpolated values of the data distribution along with uncertainties (kriging variance that accounts for the data uncertainties). By applying a weighting function based on the correlation between the data and the distance between them, the kriging method allows cancelling the effect of high density area, typically cities, where PS are more concentrated than elsewhere, notably poorly anthropized areas where the number of data points can be low. We use ordinary kriging to densify the spatial distribution of PS  
235  
240

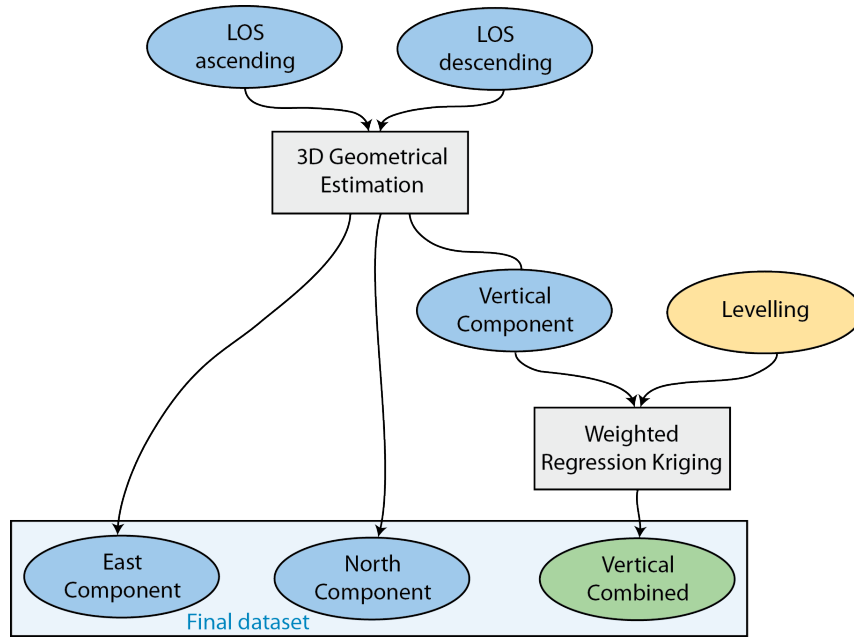


**Figure 6.** Algorithm of the two-step methodology developed to combine deformation velocities estimated from interferograms and levelling surveys. 1) 3D Geometrical estimation is performed to derive East, North and Vertical component from ascending and descending **geometry**. 2) The vertical component and levelling data are combined using a weighted regression kriging technique.

(Cressie, 1988; Yamamoto, 2005; Daya and Bejari, 2015; Ligas and Kulczycki, 2015). The associated uncertainties are given by ordinary kriging as the weighted variance of the interpolated distribution of PS.

The velocity  $v_{PS}$ , measured at each point on the ground, corresponds to the component along the radar line-of-sight (LOS) of the deformation. It contains portions of all three dimensions of the **deformation**, depending on the geometry of the acquisition and the angle between the vertical and the measured point (Catalão et al., 2009), such as:

$$v_{PS} = \mathbf{s} \cdot \mathbf{v} \quad (1)$$

where  $\mathbf{v}$  is the three dimensional vector of the deformation velocity and  $\mathbf{s}$  is the unit vector pointing from the ground towards the satellite. This unit vector is defined by the incidence angle ( $\Theta$ ), and by the look angle with respect to the North ( $\beta$ ) associated to each geometry of acquisition.

$$\mathbf{s} = \begin{bmatrix} -\sin\Theta \sin\beta \\ -\sin\Theta \cos\beta \\ -\cos\Theta \end{bmatrix} \quad (2)$$

At first order, we make the assumption that the angles of incidence are identical and that look angles for both geometries are symmetrical with respect to the North-South axis. This leads to components of the unit vectors for ascending and descending

geometries such as  $s_{asc}^n = s_{dsc}^n = -0.13$ ,  $s_{asc}^v = s_{dsc}^v = 0.82$  and  $s_{asc}^e = -s_{dsc}^e = 0.55$ . Because the maximum deformation in the area of interest is on the order of 10 to 20 mm/yr (for the North and Vertical component), this assumption induces errors ranging from 0.1 mm/yr to 0.8 mm/yr, which are one order of magnitude lower than data uncertainties. Using the components of the unit vectors for ascending and descending geometries, we can deduce the following relation to estimate the East and a near-vertical component of the deformation, such as:

$$v_e = 0.9 (v^{dsc} - v^{asc}) \quad (3)$$

$$v_u = 0.61 (v^{asc} + v^{dsc}) \quad (4)$$

By assuming that the deformation of the subsidence observed in Vauvert is radial in first approximation, we can estimate the North component of the velocity such as  $v_n = v_e \tan \alpha$  where  $\alpha$  is the angle between the E-W axis and the azimuth of the data point relative to the highest subsiding location. Due to the singularities of this function for  $\alpha$  approaching 90 and 270°, we assume that the horizontal deformation pattern is similar to vertical one. Therefore, iso-contours of velocities can be established and are centered on the highest subsiding location. The 3D components of velocity field derived from InSAR can be defined as,

$$v_e = 0.9 (v^{dsc} - v^{asc}) \quad (5)$$

$$v_n = \sqrt{(v_h^2 - v_e^2)} \quad (6)$$

$$v_u = 0.61 (v^{asc} + v^{dsc}) - v_n \quad (7)$$

where  $v_h = \frac{\pi - \alpha}{\pi} |v_{he}| + \frac{\alpha}{\pi} v_{hw}$  is the velocity in the horizontal plane of a point  $p$ .  $v_{he}$  and  $v_{hw}$  correspond to the projected velocities along the East-West profile crossing the center of subsidence. From these relations, we produce the three dimensional velocity field associated with the extraction of salt in Vauvert.

### 3.1.3 Step 2: Weighted regression kriging

In the second step of our combination approach, we use a regression-kriging method (e.g. Hengl et al. 2007) to refine the vertical velocity field in the areas where levelling data are available. Indeed, levelling surveys provide accurate measurements of the vertical velocity field, but only on a finite number of points (120). Also, levelling benchmarks are only distributed along linear paths, making the use of co-kriging inappropriate to combine InSAR and levelling data on a spatial grid. Instead, regression-kriging uses regression on auxiliary information and then uses simple kriging with known mean (0) to interpolate the residuals from the regression model (Hengl et al., 2004). This method allows to make predictions by modelling the relationships between the target and one or more auxiliary variables (the predictor(s)) at common sampling locations. In this study, we use the generic framework developed by Hengl et al. (2004) for spatial prediction of vertical velocity field. To do so, we sample the vertical velocity field from InSAR data (target data) at levelling benchmarks location (auxiliary data). Then, a linear regression of a target variable on predictors is applied with a kriging of the residuals of the prediction. Finally, we estimate a reliability index at each point of the grid, taking into account the uncertainties of each technique and the uncertainty associated with the interpolations.

285 On Figure 7a to c we represent East, North and vertical components of the **deformation** resulting from the data combination, along with their associated uncertainties (Figure 7d to f). The incorporation of levelling data in the combination allowed refining the vertical component of the deformation measured from dual geometry InSAR. The deformation induced by the salt exploitation in Vauvert is characterized by both a horizontal and vertical **deformations**. ~~Indeed,~~ compared to Raucoules et al. (2003), the combined dataset (along with GNSS velocities) **allows to identify** significant horizontal displacements. East and  
 290 North components of the velocity field indicate **a deformation with maximum deformation** towards the center of the exploitation (Parrapon site, black dots on Figure 7) of about 18 mm/yr (Figure 7a and b). The maximum vertical velocity reaches 24 mm/yr (Figure 7c) and is located above the salt exploitation of Vauvert. The subsidence affects a large area in a radius of about 3 km from the center of the exploitation (black dots on Figure 7).

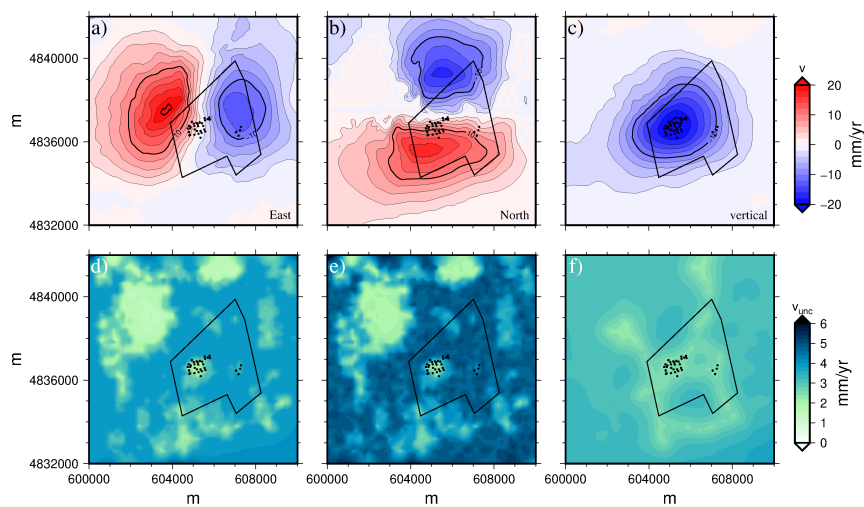


**Figure 7.** The three components (East, North and vertical) of the velocity field calculated using the two-step methodology described in this section (a to c) and their associated uncertainties (d to f). The black dots show the well locations. Black polygon is **KemOne properties** boundary.

#### 4 Multi-sources inversion

##### 295 4.1 Forward model

The salt formation lays between 1500 and 3000 m **deep in sheet-like layers dipping at  $30 \pm 5^\circ$  induced by the presence of normal faults and two décollements D1 and D2 (Valette and Benedicto 1995, Figure 1)**. We can assimilate this salt layer to a rectangular plane (Figure 1 and 8), with parameters set according to the salt layer properties (dip, azimuth). This plane covers the allochthonous saliferous unity, and extends to La Galine's boreholes (Figure 8). Previous studies (Maisons et al., 2006;  
 300 Raucoules et al., 2003, 2004) have highlighted a quasi-perfect spherical bowl of subsidence in Vauvert originated from the

exploitation of this salt formation. In this study, the combined dataset (Figure 7) shows a consistent vertical signal but also provides horizontal displacements. **To infer the deep deformation using this combined dataset, the single dislocation plane is not sufficient to explain the horizontal motion.** Hence, we subdivide the single rectangular plane into 21 square planes of 1 km side at fixed location and orientation with respect to the salt layer characteristics (Figure 8). Such discretization is necessary to model vertical and horizontal velocities, but also to identify any model boundary effects that may occur (difficult to obtain with a coarser discretization). Finer discretization implies more computational work, needs regularization to avoid sharp variations between one plane to another, and the degree of freedom is out of range of the mean resolution of surface measurements.

The forward model uses three dimensional, elastic dislocation theory in a homogeneous half space (Okada, 1992). In the case of Vauvert's exploitation, using an elastic model **allows to give an** acceptable approximation of the deformation induced by the brine extraction **during two years of monitoring**, unlike what salt creeping would do at this time scale. Each plane has its own independent strike-slip, dip-dip and tensile components, such as both the rapid depletion at the vicinity of the exploiting wells and the creeping deformation in the salt layer can be considered. Planes are dipping at 30° towards the North-West (N 50) and extent from 1500 to 3000 m deep. Top of the planes (1500 m deep) is identified with the thick orange line on Figure 8. Most of the exploitation wells (red dots on Figure 8) are located on Parrapon site and are mainly gathered inside one plane of the model. La Galine's wells are partly drained (two wells) and therefore **not producing** much brine during the considered time.

In this model, we consider 63 free dislocations parameters to be retrieved by inverting the combined dataset, fixing all other parameters of the planes (positions, orientations, dimensions). Hence, the Green's functions describing the analytical solution for the surface displacements  $\mathbf{v}$  (Okada, 1992) are linear with the dislocation parameters:

$$\mathbf{v} = \sum_{i=1}^{21} \sum_{j=1}^3 U_j^i \boldsymbol{\alpha}_j^i \quad (8)$$

where  $U_j^i$  are the dislocation type  $j$  (strike 1, dip 2 or tensile 3) associated **to** each plane  $i$  and  $\boldsymbol{\alpha}_j^i$  are three-dimensional vectors between the point at the surface where  $\mathbf{v}$  is sought, and the dislocation at depth.

## 4.2 Inversion strategy

**The dislocations parameters are set free to vary between -1 and 1 m** throughout the inversion process. Initialized with no a priori information, a first modelled dataset is produced which is compared to the observations. We choose to build the functional as the weighted Euclidian norm of the residual vector  $\mathbf{D}$  between observed and modeled dataset:

$$J = \mathbf{D}^T \boldsymbol{\Sigma}^{-1} \mathbf{D} \quad (9)$$

where  $\boldsymbol{\Sigma}$  is the data covariance matrix associated **to** each point of the dataset, and  $^T$  denotes the transpose of the residual vector. Through this formulation of the functional, we consider the resolution of the measurement: for highly uncertain data, their covariance matrix is large compared to the data values, leading to small values of  $J$ . This functional needs to be lower than the data uncertainties or **reach** a minimum value for the optimization to be complete. This linear problem (Eq. 8) is

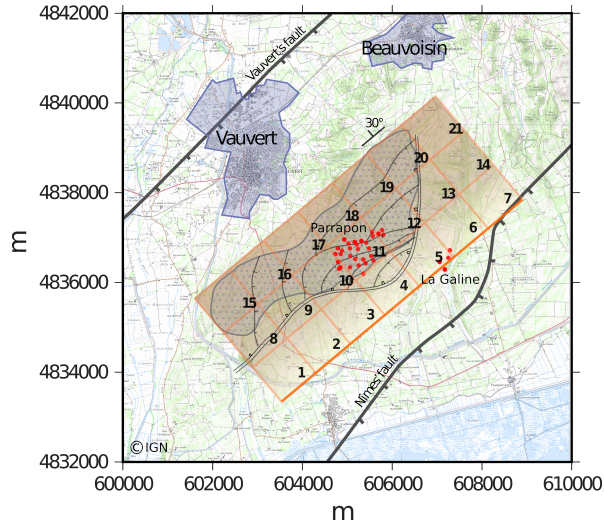


**Figure 8.** Location of the **décollement** (double line) and listric faults beneath the site of salt exploitation in Vauvert (France). The allochthonous saliferous unity is represented by the gray dotted area. The limits of Vauvert and Beauvoisin cities are represented by blue areas and Vauvert and Nîmes normal faults are displayed using black lines (modified from Valette and **Benedicto 1995**). The dislocation planes (numbering from 1 to 21) are overlaid on this map in shaded orange (darker shading for deeper planes), along with the current known boreholes (red dots). The background map is extracted from IGN SCAN 1:25000 (©IGN).

solved using an optimization algorithm **allowing to process** problem with non-linear relations. By doing so, we can easily switch to a different forward model, including more complex and realistic physics without implementing a new optimization approach. Our optimization process is based on a recursive algorithm defining a multi-criteria global optimization, varying not only the parameters of the model, but also the initial **guesses** (Ivorra and Mohammadi, 2007; Mohammadi and Pironneau, 2009). This **allows to ensure** that **a given set of optimal model parameters realizes the global minimum of the functional**. To determine the model parameters uncertainties, we implement the approach developed by Mohammadi (2016) using backward uncertainty propagation. This approach is based on the introduction of directional quantile-based extreme scenarios knowing the probability density function of the target data. By doing so, we avoid to compute numerous scenarios of data perturbation to generate probability density function (PDF) of a functional  $J$ . Instead, we use the sensitivity of the functional with respect to the data and explore only the optimal region given by the optimization to identify two directional extreme sets of data. Two datasets  $v_i^\pm$  are obtained by perturbing observed data  $v_i$  knowing the associated data uncertainty  $\sigma_i$  along the direction given by residual value between optimal and observed data  $v_i^* - v_i$  (the fractional term is unit).

$$v_i^\pm = v_i \pm 1.65 \sigma_i \frac{v_i^* - v_i}{\|v_i^* - v_i\|} \quad (10)$$

The maximum and minimum deviations for the optimal solution of the inversion due to the uncertainty of the data are hence given by the two extreme **scenarios**.

### 4.3 Results of the inversion

#### 4.3.1 Parameters and resolution analysis

The inversion leads to a distribution of strike-slip, dip-slip and tensile dislocations associated to each plane of the model (black dots on Figure 9a to c). We estimate the upper and lower admissible value associated (at  $2\text{-}\sigma$ ) to each dislocation parameter, using the directional extreme scenarios as previously described. The blue and red dots on Figure 9a to c stand for the two extreme scenarios ( $v^+$  and  $v^-$  respectively). In both scenarios, the distributions remain close to the optimal solution. By calculating the difference between the optimal solution and each scenario, we compute the range of confidence for each parameter. These confidence intervals are on the order of several centimeters (up to 10 cm for the largest intervals). For instance, the plane containing most of the exploitation wells (plane 11) is closing at a value between 30.9 and 38.6 cm at  $2\text{-}\sigma$ . This means that the solution obtained from the inversion is robust and is the best we can get with respect to the data and their uncertainties. If confidence intervals include zero-deformation (with respect to parameter uncertainties), then we can say that the determined displacement is not significant at  $2\text{-}\sigma$ .

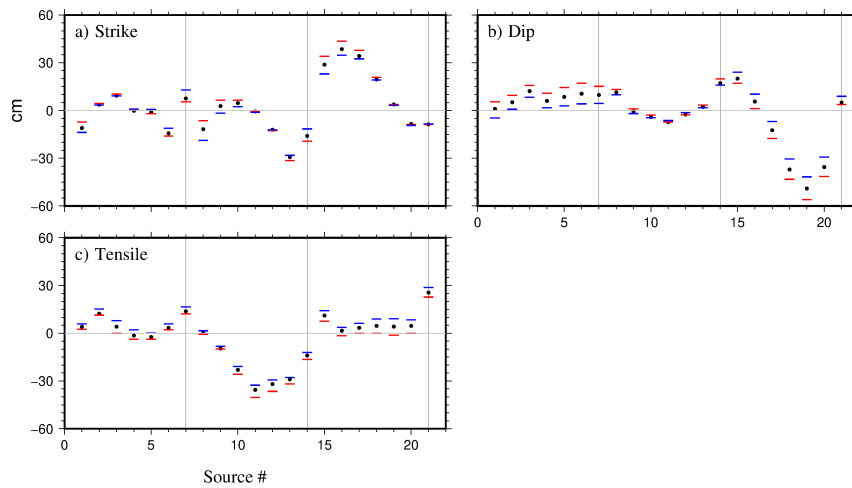


**Figure 9.** Interval of confidence ( $2\text{-}\sigma$ ) for the dislocation parameters of the 21 sources: a) strike slip, b) dip-slip and c) tensile. The black dots represent the optimal value of the parameter, red and blue are associated with the two extreme scenarios ( $v^+$  and  $v^-$  respectively) obtained using the backward uncertainty propagation previously described. The black lines on the graphs separate the sources contained in the three lines that composed the model. The grey line indicates zero deformation of the plane.

We represent the distribution of dislocation values associated to each plane on Figure 10. The planes where the displacement is not significant are colored in grey. From Figure 10a, b and d, one can observe that most of the slip motion occurs on the deepest planes. The strike-slip motions range from  $-29.3$  to  $38.5$  cm while dip-slip motions range from  $-49.0$  to  $20.0$  cm. Figure 10d displays the slip vectors of the hanging wall relative to the foot wall. The slip indicates a rotational motion from the external planes towards North-East of the exploitation (black dots stands for the well heads). Figure 10c shows that tensile motion near

the exploitation is mainly due to closure of planes (from -35.6 to -1.4 cm). Nevertheless, some opening also occurs on half of  
 365 the planes (ranging from 0.32 to 25.6 cm). Tensile motions of planes seem to be related to the plane depth:

- Planes 1 to 7 are the shallowest (the center of the planes are at -1750 m deep). Significant displacements show small opening (positive values of tensile motion) with a mean value of 8.4 cm.
- Planes 8 to 14 are located right beneath the extracting wells (-2250 m deep) and record a mean closure of -23.8 cm.
- Planes 15 to 21 are the deepest planes (-2750 m deep) and are recording the most negligible deformation (planes 16 to  
 370 20) but also openings located on both planes 15 and 21 (11.1 and 25.6 cm respectively).

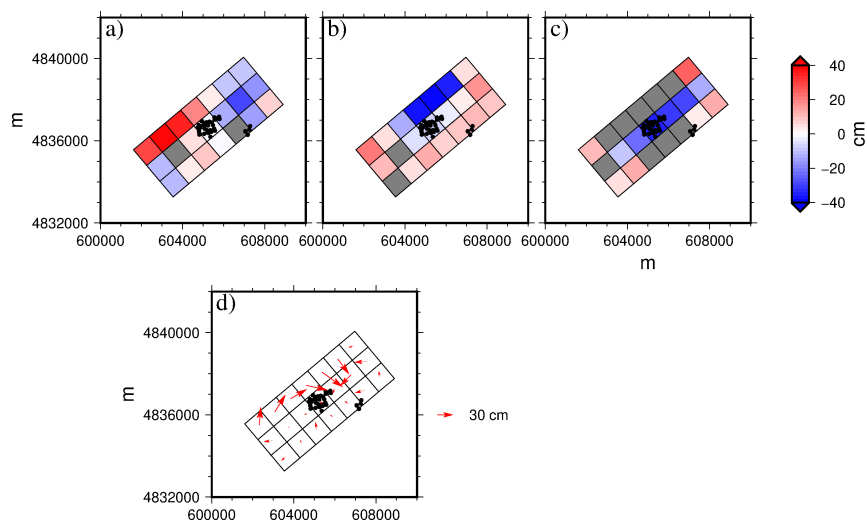


**Figure 10.** Distribution of the significant optimal dislocation parameters: a) strike-slip, b) dip-slip c) tensile and d) slip displacement (strike and dip) of the hanging wall relative to the foot wall. The black dots indicate the location of well heads. Non-significant dislocations are represented in grey.

### 4.3.2 Residuals

The optimal set of dislocation parameters produces a modelled deformation (Figure 11a to c) that can be compared to the obser-  
 vations (Figure 7). On Figure 11d to f, we represent the norm of the residual signal for each velocity component (respectively  
 375 East, North and Vertical). These residuals correspond to the differences between the observed and modeled data. The mean residual values are 1.8 mm/yr, 2.5 mm/yr and 1.6 mm/yr for East, North and vertical component, but maximum residuals reach 9.0 mm/yr, 10.8 mm/yr and 8.3 mm/yr respectively. For the East component (Figure 11a), the general shape of the deformation seems to be retrieved by the inversion, while the amplitude of the velocities is underestimated by the model: high residuals (>5 mm/yr) are localised North-East of the model and above planes 12 to 14 and 19 to 21 (Figure 11d) and moderate residuals (between 2 to 5 mm/yr) are observed above planes 3 and 4. The North component of the signal is the less well retrieved of

380 all three. Large areas with high residuals are observed above and North of the exploitation (Figure 11e). The amplitude of the signal is also underestimated by the inversion. The vertical component presents the best fit to the observed data with only small areas of moderate (above planes 1, 3 and 7) to high residuals (North of planes 18 and 19). These areas of moderate to high residuals correspond to more uncertain data for the corresponding component (Figure 7d to f).

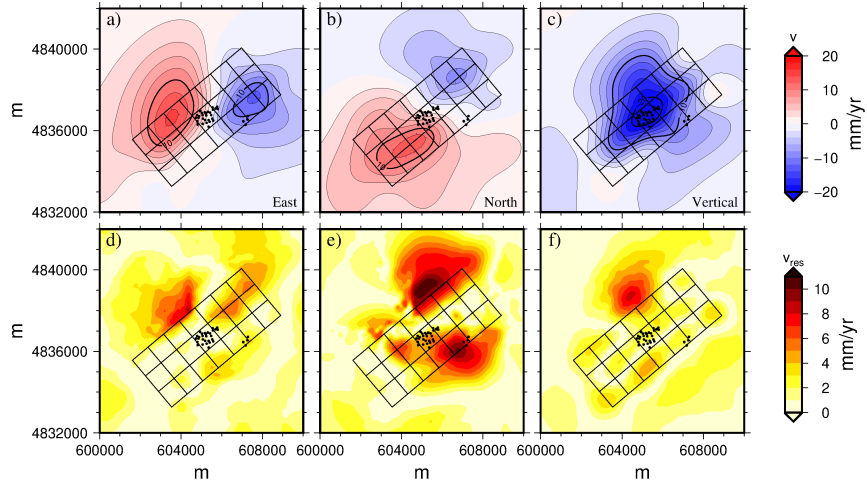


**Figure 11.** a) East, b) North and c) vertical components of the deformation from the optimal model with the associated residuals (d, e and f respectively). The mean values of residual norms are estimated to 1.8 mm/yr, 2.5 mm/yr and 1.6 mm/yr for East, North and vertical component respectively.

The fit between the observed and modelled signals is estimated using the normalized RMS (*NRMS*) (McCaffrey, 2005):

$$385 \quad NRMS = \left[ N^{-1} \left( \sum_{i=1}^N r_i^2 / \sigma_i^2 \right) \right]^{1/2} \quad (11)$$

where  $N$  is the number of observations,  $r$  is the residual and  $\sigma$  is the data uncertainty. This unitless level indicates if the modelled data fit the observation with respect to data uncertainties and should be close to 1. Besides, we can also compute the weighted RMS (*WRMS*) from McCaffrey (2005) which gives an estimation of the a posteriori weighted scatter in the fit.

$$WRMS = \left[ \left( \sum_{i=1}^N r_i^2 / \sigma_i^2 \right) / \left( \sum_{i=1}^N 1 / \sigma_i^2 \right) \right]^{1/2} \quad (12)$$

390 In this work, the level of fit for our dataset is  $NRMS=0.8$  and a posteriori scatter is  $WRMS=2.7$  mm/yr (to be compared to the mean uncertainty value of 3.6 mm/yr). Separating the horizontal and the vertical velocities leads to values of *WRMS* of 3.36 mm/yr and 1.1 mm/yr respectively.

## 5 Discussion

The combination of ascending, descending and levelling data produces a 3-D velocity field measuring the deformation above the salt exploitation of Vauvert. The vertical velocity computed through this process is fairly similar to the one estimated by Raucoules et al. (2003). Differences may notably stem from both the period of interest (different) and the incorporation of levelling data (as opposed to stand alone InSAR). In Table 1, we compare the three components of the velocity field derived from the dual InSAR geometry/levelling combined set to their GNSS counterparts. Although the values from the combined set seem to overestimate the horizontal velocity, they underestimate most of the vertical velocity. The differences between both methods of deformation measurement are given by the residuals in Table 1 and can partly be explained by different time coverages of the methods. Another source for such differences is probably linked to the hypotheses assumed for the combination. Indeed, the highest residuals are observed for the north and vertical components (with mean values of 3.4 and 4.9 mm/yr respectively) whereas the east component of the combined set seems to better fit the GNSS data (2.5 mm/yr). North and vertical velocities are strongly correlated (Eq. 6 and 7) and the deformation is considered to be purely radial. However, performing an inversion with very low constrain on the North component leads to non-unique solutions for the optimization parameters and high residuals. Indeed, the inversion results suggest that the deformation may not be completely radial. This demonstrates the importance of data combination, not only to better constrain the vertical component, but also the three dimensions of the deformation. And to improve this 3-D field, including GNSS data in the combination would be extremely recommendable. As a result, a more detailed interpretation of the dislocations would be possible, including creep and loading (or not) of the surrounding faults.

**Table 1.** Three components of the deformation from GNSS and the Dual InSAR geometry / levelling combined dataset observed at GNSS locations, and their residuals.

Stations	GNSS			Combined data			Residuals		
	$v_e$ (mm/yr)	$v_n$ (mm/yr)	$v_u$ (mm/yr)	$v_e$ (mm/yr)	$v_n$ (mm/yr)	$v_u$ (mm/yr)	$r_e$ (mm/yr)	$r_n$ (mm/yr)	$r_u$ (mm/yr)
VAU1	0.2	5.2	-3.0	1.6	11.3	-4.1	1.5	6.1	1.1
VAU2	-3.2	-10.4	-17.9	-7.8	-13.3	-9.0	4.7	2.9	8.9
VAU3	-9.4	3.6	-13.8	-12.9	4.2	-10.2	3.5	0.5	3.6
VAUV	5.9	-1.6	-25.8	5.4	2.5	-19.9	0.6	4.1	5.9

The methodology of combination requires specific conditions (see Section 3.1.1) among which, the most restrictive are the adequacy of the periods of time considered for each technique, the radial-shaped deformation and, depending on the exact goals of the combination (e.g. horizontal components or not), sufficient density of measurements. Hence, applications of the 2-step process is conceivable in areas where the observed deformation is near-radial such as in gas storage, solution mining or filling and draining of magmatic chambers.

In addition, we check our model using the available GNSS data (red arrows on Figure 12a and b). We model the velocity at the 4 GNSS stations (green arrows on Figure 12a and b) and compare it to the observations. The differences between observed and modeled data are represented on Figure 12c and d for the horizontal and vertical velocities respectively (note the change in arrow scale compared to Figure 12a and b). We estimate  $NRMS=11.6$  and  $WRMS=1.4$  mm/yr for the horizontal velocity while  $NRMS=12.5$  and  $WRMS=4.1$  mm/yr for the vertical velocity. The level of correlation between the combined solution and its GNSS-only counterpart is obviously low. This may be due to the very small uncertainties associated with GNSS velocities (typical of continuous GNSS) and to the difference between the periods considered (GNSS time series cover 2 to 4 years with only 1.5 years overlap with the InSAR process). In East and North component, this may also and mostly be due to the relative location of the GNSS stations within the subsidence bowl. InSAR can hardly yield accurate horizontal deformation on specific spots unless they are optimally located (e.g. VAU3 in East, VAU2 in North), assuming that the period of interest is sufficient (1.5 years overlap are short). Therefore, the global amplitude of the deformation may be preserved, but the shape may have evolved with the exploitation migrating northward. Given the high residuals between GNSS and combined dataset, the combination would certainly improve the results. Hence, with a complete overlap of the GNSS data with InSAR and levelling data, we could use the 3-D velocity field from the GNSS data in the combination process, by readjusting InSAR over the 3 dimensions, independently for both ascending and descending geometries.

The inversion of the combined velocities allow to constrain at first order, the displacements of the salt layer using an elastic model made of 21 planes of dislocation. The global slip displacement (Figure 10d) indicates an overall first order motion of the outer and deeper planes toward the center of the model where the salt exploitation is. In our case, it can be due to the fact that wells are highly connected, implying a salt flow (or short term creep) from the entire layer towards the center of the exploitation where there is a strong change in pressure and large cavities opened in the salt layer. Tensile motions mainly show a subsidence of the central planes (from 8 to 14) with a maximum collapse of 35.6 cm/yr at plane 11. From the model, we estimate a volume of 537 000 m<sup>3</sup> corresponding to a mass of 1.16 million tons per year of extracted salt. This is in agreement with the real mass of extracted salt of about 1 million tons of brine every year at 2 km depth (1.0 million tons in 2015, 0.93 million tons in 2016 and 1.08 million tons in 2017). The strong collapse observed at plane 11 is hence produced by the high pumping rate at extracting wells. Besides, at such depth, wells are drilled through a system of normal faults (Figure 1). This means that openings (occurring at planes 1, 2, 6, 7, 15, 21 see Figure 10) could potentially be explained by the motions along normal faults.

This model is the best we have found considering the available datasets and their uncertainties. A series of alternative models have also been computed to make sure that the selected model was optimal. For instance, we vary the dip of the salt layer and set it to 25° and 35°. Considering these values of dip leads to a distribution of parameters whose amplitudes fit, within a scalar factor, the ones from the model presented in this paper, but with higher residuals. Increasing the number of planes to 28 in the model by adding a fourth row deeper does not significantly improve the residuals either. The optimal number of planes was found out by trial and error. Okada's model offers a simple model to test at first if the surface deformation is only related to subsidence at depth due to the extraction of salt or if creep occurs in the salt layers. Based on our model, creep occurs in the salt layers, the next step would be to produce a more global model, with an increase in the level of complexity by considering 1) strain source

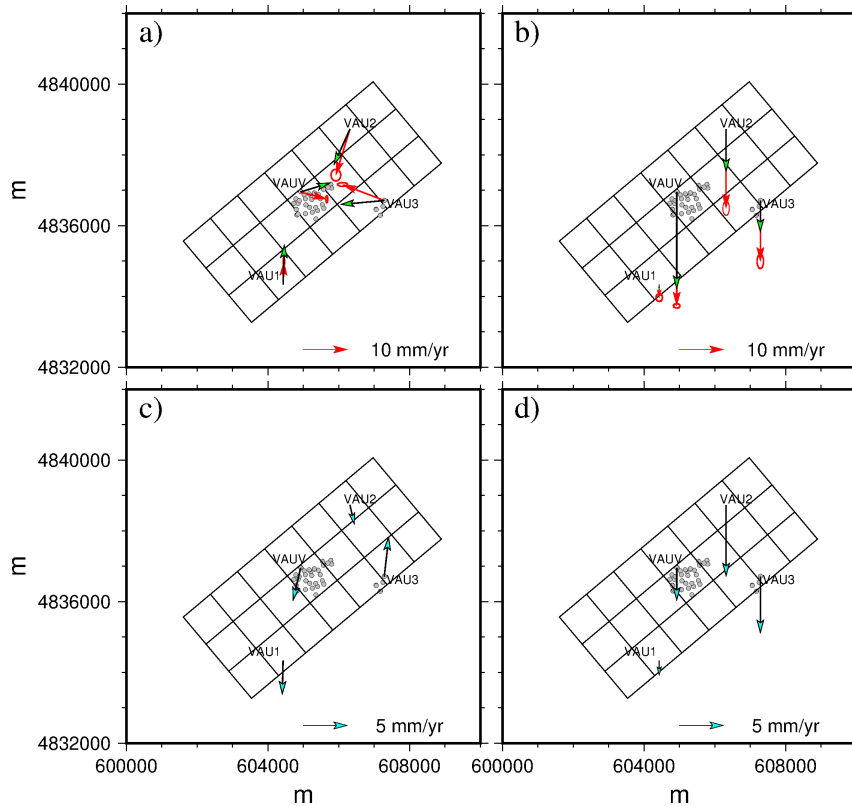


**Figure 12.** a) Horizontal and b) vertical velocities at the 4 permanent GNSS stations. Red arrows stand for the observed data and their  $2\text{-}\sigma$  uncertainties and green ones for the modelled velocities using optimal parameters. c) and d) represent the associated residuals. Note the change in arrow scale compared to a and b.

with 6 free parameters which generate a volumetric and shear deformation (Furst et al., 2020), 2) elasto-viscoplastic laws to include salt creep, 3) finite elements to discretize the domain.

The model constrained by the inversion of geodetic data **allows to estimate** stress tensor. This modelled tensor could be compared to in-situ horizontal stress orientations from the analysis of borehole breakout. They generally occur at the azimuth  
 455 of the minimum horizontal stresses and perpendicular to the maximum horizontal stress. These borehole failures are generated by compressive failure of the borehole wall and result in its enlargement in the minimum horizontal stress direction. Several logs were conducted in some of Vauvert's exploitation wells and need to be analysed. Comparing the modelled and observed stresses would permit to assess the reliability of our model. The Nîmes and Vauvert faults are part of the fault system that ruptured with a Mw 4.9 earthquake on November 11th 2019 (Ritz et al.). This earthquake hypocenter was very shallow and  
 460 might have been partially triggered by a limestone quarry in activity over the last 100 years (Ampuero et al., 2020). Given that the site seems to experience the same regional strain pattern (Masson et al., 2019), it would be important to estimate the effect of the salt creep on the stress state of the surrounding faults.

The microseismic activity of the exploitation was monitored between 1992 and 2007 with magnitude events ranging from -0.5 to 3 (Godano, 2009; Godano et al., 2010, 2012). Seismic activity either occurs at the **décollement** depth for abandoned doublets or at **depths** of production zones for active doublets. Nowadays, a new network has been deployed by the **french** company Magnitude to monitor the microseismicity of the site both for the brine exploitation and for hazard management. Using the model developed in this study and the seismic events, we could also calibrate rheological law in the area of the salt exploitation.

## 6 Conclusions

470 We developed a 2-step methodology combining ascending and descending LOS with levelling data in order to overcome the difference of resolution and accuracy associated with the measurement methods. This process is specific to near-radial deformation measured by geodetic techniques whose periods of observation are consistent with each other and whose density in space and time are adequate to achieve the monitoring goals (only vertical or also horizontal). The incorporation of levelling data allowed refining the InSAR-derived deformation in height. Satellite lines of sight and flight directions must also be  
475 symmetrical enough from one acquisition geometry to the other, to extract the East-component of the deformation in first approximation. The resulting 3-D velocity field gives a spatially dense measure of the deformation whose uncertainties are all the most reliable in those areas covered by several geodetic techniques. Due to their period of availability, slightly shifted and quite short, GNSS stations could only provide a control in first approximation. Along with the salt layer modelling, this result demonstrated the great interest for combining timely-compliant geodetic measurements with InSAR.

480 We inverted this combined dataset to constrain a kinematic model of the salt layer. Because we focus on a two-years interval for the dataset, the deformation induced by the extraction is largely dominating the salt creep and an elastic model is acceptable. Hence, we proposed to assimilate the salt layer to a collection of 21 planes of dislocation with fixed positions, geometries and orientations consistently with the salt layer characteristics. The results of the inversion indicate a collapse of the planes located beneath the exploitation and the adjacent ones at the same depth. We also identified a salt flow from the deepest and most  
485 external part of the salt layer towards the center of the exploitation due to the connections between the wells and the exploited layer. Although this model gives a first approximation of the deep deformation of the salt layer, it needs to be improved to be able to predict the deformation induced by the exploitation in the future. We suggest three levels of model improvements, involving a collection of strain sources or finite elements and elasto-viscoplastic laws for the long-term prediction.

*Code and data availability.* The geodetic dataset processed and combined in the work as well as the optimization code are available on  
490 request from the corresponding author.

*Author contributions.* S.D. developed the concept of geodetic data combination under the supervision of P.V., C.C. and J-L.C. S.D. performed the two-step combination of InSAR and levelling data. S.F. built the inversion algorithm based on available global optimization code. S.F. designed and performed the numerical calculations for the experiments. S.F. wrote the manuscript and designed the figures with the support of S.D., P.V., C.C. and J-L.C.

495 *Competing interests.* The authors declare no competing interests.

*Acknowledgements.* The authors want to thank KemOne company for sharing production data and for allowing the installation of various instruments on the site, and more specifically Marc Valette for sharing the geological information essential to build and interpret the model presented in the paper. We also thank Jean Chéry, Michel Peyret, Bijan Mohammadi and Jean-Luc Got for the inspiring discussions, their advices and insightful comments.

## 500 **References**

- Abidin, H., Andreas, H., Gumilar, I., Yuwono, B., Murdohardono, D., and Supriyadi: On Integration of Geodetic Observation Results for Assessment of Land Subsidence Hazard Risk in Urban Areas of Indonesia, *International Association of Geodesy Symposia*, pp. 145–153, <https://doi.org/10.1007/1345>, 2015.
- Ampuero, J.-P., Billant, J., Brenguier, F., Cavalié, O., Courboux, F., Deschamps, A., Delouis, B., Grandin, R., Jolivet, R., and Liang, C.:  
505 The November 11 2019 Le Teil, France M5 earthquake : a triggered event in nuclear country, in: *EGU General Assembly*, 2020.
- Astakhov, D. K., Roadarmel, W. H., Nanayakkara, a. S., and Service, H.: SPE 151017 A New Method of Characterizing the Stimulated Reservoir Volume Using Tiltmeter-Based Surface Microdeformation Measurements, in: *SPE Hydraulic Fracturing Technology Conference*, pp. 1–15, The Woodlands, Texas, 2012.
- Bato, M. G., Pinel, V., and Yan, Y.: Assimilation of Deformation Data for Eruption Forecasting: Potentiality Assessment Based on Synthetic  
510 Cases, *Frontiers in Earth Science*, 5, 1–23, <https://doi.org/10.3389/feart.2017.00048>, <http://journal.frontiersin.org/article/10.3389/feart.2017.00048/full>, 2017.
- Bérest, P. and Brouard, B.: Safety of salt caverns used for underground storage blow out; mechanical instability; seepage; cavern abandonment, *Oil & Gas Science and Technology*, 58, 361–384, <https://doi.org/10.2516/ogst:2003023>, 2003.
- Bérest, P., Karimi-jafari, M., Brouard, B., Bazargan, B., Mécanique, L. D., Polytechnique, E., and Consulting, B.: In situ mechanical tests in  
515 salt caverns, in: *Solution Mining Research Institute*, pp. 1–39, Brussels, Belgium, 2006.
- Bérest, P., Djakeun-djizanne, H., Brouard, B., and Hévin, G.: Rapid Depressurizations : Can they lead to irreversible damage ?, in: *SMRI SMRI Spring Conference*, pp. 63–86, Regina, 2012.
- Burdack, J.: Combinaison des techniques PSinSAR et GNSS par cumul des équations normales, Ph.D. thesis, Conservatoire National des Arts et Métiers - Ecole Supérieure des Géomètres et Topographes, 2013.
- 520 Camacho, A. G., González, P. J., Fernández, J., and Berrino, G.: Simultaneous inversion of surface deformation and gravity changes by means of extended bodies with a free geometry: Application to deforming calderas, *Journal of Geophysical Research: Solid Earth*, 116, 1–15, <https://doi.org/10.1029/2010JB008165>, 2011.
- Catalão, J., Nico, G., Hanssen, R., and Catita, C.: Integration of Insar and Gps for Vertical Deformation Monitoring : a Case Study in Faial and Pico Islands, *Proc. 'Fringe 2009 Workshop'*, Frascati, Italy, pp. 1–7, 2009.
- 525 Colombo, D., Mantovani, M., Stefano, M. D., De Stefano, M., Garrad, D., and Al-Lawati, H.: Simultaneous Joint Inversion of Seismic and Gravity Data for Long Offset Pre-Stack Depth Migration in Northern Oman, *CSPG CSEG Convention*, 41569, 191–195, <http://www.cseg.ca/conventions/abstracts/2007/2007abstracts/053S0129.pdf>, 2007.
- Comerci, V. and Vittori, E.: The need for a standardized methodology for quantitative assessment of natural and anthropogenic land subsidence: The Agosta (Italy) gas field case, *Remote Sensing*, 11, <https://doi.org/10.3390/rs11101178>, 2019.
- 530 Cressie, N.: Spatial prediction and ordinary kriging, *Mathematical Geology*, <https://doi.org/10.1007/BF00892986>, 1988.
- Daya, A. A. and Bejari, H.: A comparative study between simple kriging and ordinary kriging for estimating and modeling the Cu concentration in Chehlkureh deposit, SE Iran, *Arabian Journal of Geosciences*, 8, 8263–8275, <https://doi.org/10.1007/s12517-014-1618-1>, 2015.
- Donadei, S. and Schneider, G. S.: Compressed Air Energy Storage in Underground Formations, in: *Storing Energy: With Special Reference to Renewable Energy Sources*, edited by Trevor M. Letcher, chap. Chapter 6, pp. 113–133, Elsevier, <https://doi.org/10.1016/B978-0-12-803440-8.00006-3>, 2016.

- Doucet, S.: Combinaison de mesures géodésiques pour l'études de la subsidence : application à la saline de Vauvert (Gard, France), Ph.D. thesis, University of Montpellier, 2018.
- 540 Farr, T. G. and Kobrick, M.: Shuttle radar topography mission produces a wealth of data, *Eos*, 81, 583–585, <https://doi.org/10.1029/EO081i048p00583>, 2000.
- Farr, T. G., Rosen, P. A., Caro, E., Crippen, R., Duren, R., Hensley, S., Kobrick, M., Paller, M., Rodriguez, E., Roth, L., Seal, D., Shaffer, S., Shimada, J., Umland, J., Werner, M., Oskin, M., Douglas, B., and Alsdorf, D.: The shuttle radar topography mission, *Review of geophysics*, 45, <https://doi.org/10.1029/2005RG000183>.1.INTRODUCTION, 2007.
- 545 Fokker, P. A., Visser, K., Peters, E., Kunakbayeva, G., and Muntendam-Bos, A. G.: Inversion of surface subsidence data to quantify reservoir compartmentalization: A field study, *Journal of Petroleum Science and Engineering*, 96-97, 10–21, <https://doi.org/10.1016/j.petrol.2012.06.032>, 2012.
- Fuhrmann, T., Caro Cuenca, M., Knöpfler, A., van Leijzen, F. J., Mayer, M., Westerhaus, M., Hanssen, R. F., and Heck, B.: Estimation of small surface displacements in the Upper Rhine Graben area from a combined analysis of PS-InSAR, levelling and GNSS data, *Geophysical Journal International*, 203, 614–631, <https://doi.org/10.1093/gji/ggv328>, 2015.
- 550 Furst, S., Chéry, J., Peyret, M., and Mohammadi, B.: Tiltmeter data inversion to characterize a strain tensor source at depth: application to reservoir monitoring, *Journal of Geodesy*, <https://doi.org/10.1007/s00190-020-01377-5>, 2020.
- Galgana, G. A., Newman, A. V., Hamburger, M. W., and Solidum, R. U.: Geodetic observations and modeling of time-varying deformation at Taal Volcano, Philippines, *Journal of Volcanology and Geothermal Research*, 271, 11–23, <https://doi.org/10.1016/j.jvolgeores.2013.11.005>, <http://www.sciencedirect.com/science/article/pii/S0377027313003326>, 2014.
- 555 Geirsson, H., La Femina, P. C., Sturkell, E., Ofeigsson, B., Arnadóttir, T., Hooper, A. J., Lund, B., Schmidt, P., Sigmundsson, F., and Affiliation: Joint Inversion of GPS, InSAR, Tilt, and Borehole Strain Data from the 2000 Eruption of Hekla Volcano, Iceland, in: *AGU 2014*, 1, pp. 1–5, <https://doi.org/10.1007/s13398-014-0173-7.2>, 2014.
- Gillhaus, A. and Horvath, P. L.: Compilation of geological and geotechnical data of worldwide domal salt deposits and domal salt cavern fields, *Solution Mining Research Institute and KBB Underground Technologies GmbH*, 2008.
- 560 Godano, M.: Etude théorique sur le calcul des mécanismes au foyer dans un réservoir et application à la sismicité de la saline de Vauvert (Gard), Ph.D. thesis, Université Nice Sophia Antipolis, 2009.
- Godano, M., Gaucher, E., Bardainne, T., Regnier, M., Deschamps, A., and Valette, M.: Assessment of focal mechanisms of microseismic events computed from two three-component receivers: Application to the Arkema-Vauvert field (France), *Geophysical Prospecting*, 58, 775–790, <https://doi.org/10.1111/j.1365-2478.2010.00906.x>, 2010.
- 565 Godano, M., Bardainne, T., Regnier, M., Deschamps, A., and Valette, M.: Spatial and temporal evolution of a microseismic swarm induced by water injection in the Arkema-Vauvert salt field (southern France), *Geophysical Journal International*, 188, 274–292, <https://doi.org/10.1111/j.1365-246X.2011.05257.x>, 2012.
- Hammond, W., Lib, Z., and Plaga, H.: Integrated Insar and Gps Studies of Crustal Deformation in the Western Great Basin, Western United States, *International Archives of ...*, XXXVIII, 39–43, <http://www.nbmj.unr.edu/staff/pdfs/JTS31{ }20100322074448.pdf>, 2010.
- 570 Hastaoglu, K. O., Poyraz, F., Turk, T., Yilmaz, I., Kocbulut, F., Demirel, M., Sanli, U., Duman, H., and Balik Sanli, F.: Investigation of the success of monitoring slow motion landslides using Persistent Scatterer Interferometry and GNSS methods, *Survey Review*, 50, 475–486, <https://doi.org/10.1080/00396265.2017.1295631>, <http://dx.doi.org/10.1080/00396265.2017.1295631>, 2017.
- Hengl, T., Heuvelink, G. B., and Stein, A.: A generic framework for spatial prediction of soil variables based on regression-kriging, *Geoderma*, 120, 75–93, <https://doi.org/10.1016/j.geoderma.2003.08.018>, 2004.

- 575 Hengl, T., Heuvelink, G. B., and Rossiter, D. G.: About regression-kriging: From equations to case studies, *Computers and Geosciences*,  
<https://doi.org/10.1016/j.cageo.2007.05.001>, 2007.
- Herring, T. A., King, R. W., Floyd, M. A., and McClusky, S. C.: Introduction to GAMIT/GLOBK, Release 10.6, Tech. rep., Massachusetts  
Institute of Technology, 2015.
- Hesse, M. a. and Stadler, G.: Joint inversion in coupled quasi-static poroelasticity, *Journal of Geophysical Research: Solid Earth*, 119,  
580 1425–1445, <https://doi.org/10.1002/2013JB010272>, 2014.
- Hooper, A., Zebker, H., Segall, P., and Kampes, B.: A new method for measuring deformation on volcanoes and other natural terrains using  
InSAR persistent scatterers, *Geophysical Research Letters*, 31, 1–5, <https://doi.org/10.1029/2004GL021737>, 2004.
- Ivorra, B. and Mohammadi, B.: Semi-deterministic global optimization method, *Journal of Optimization, Theory and Applications*, 135,  
549–561, <https://doi.org/DOI> <https://doi.org/10.1007/s10957-007-9251-8>, <https://link.springer.com/article/10.1007/s10957-007-9251-8>,  
585 2007.
- Karila, K., Karjalainen, M., Hyypä, J., Koskinen, J., Saaranen, V., and Rouhiainen, P.: A comparison of precise leveling and Persistent  
Scatterer SAR Interferometry for building subsidence rate measurement, *ISPRS International Journal of Geo-Information*, 2, 797–816,  
<https://doi.org/10.3390/ijgi2030797>, 2013.
- Ligas, M. and Kulczycki, M.: Kriging approach for local height transformations, *Geodesy and Cartography*, 63, 25–37,  
590 <https://doi.org/10.2478/geocart-2014-0002>, 2015.
- Lu, C. H., Ni, C. F., Chang, C. P., Yen, J. Y., and Hung, W. C.: Combination with precise leveling and PSInSAR observations to quantify  
pumping-induced land subsidence in central Taiwan, *Proceedings of the International Association of Hydrological Sciences*, 372, 77–82,  
<https://doi.org/10.5194/piahs-372-77-2015>, 2015.
- Lundgren, P., Hetland, E. A., Liu, Z., and Fielding, E. J.: Southern San Andreas-San Jacinto fault system slip rates estimated from earthquake  
595 cycle models constrained by GPS and interferometric synthetic aperture radar observations, *Journal of Geophysical Research: Solid Earth*,  
114, 1–18, <https://doi.org/10.1029/2008JB005996>, 2009.
- Maisons, C., Raucoules, D., and Carnec, C.: Monitoring of slow ground deformation by satellite differential radar-interferometry . A reference  
case study ., in: *Solution Mining Research Institute*, pp. 1–10, Brussels, 2006.
- Masson, C., Mazzotti, S., Vernant, P., and Doerflinger, E.: Extracting small deformation beyond individual station precision  
600 from dense Global Navigation Satellite System (GNSS) networks in France and western Europe, *Solid Earth*, 10, 1905–1920,  
<https://doi.org/10.5194/se-10-1905-2019>, 2019.
- McCaffrey, R.: Block kinematics of the Pacific-North America plate boundary in the southwestern United States from inversion of GPS,  
seismological, and geologic data, *Journal of Geophysical Research: Solid Earth*, 110, 1–27, <https://doi.org/10.1029/2004JB003307>, 2005.
- Mohammadi, B.: Backward uncertainty propagation in shape optimization, *International Journal for Numerical Methods in Fluids*, 80, 285–  
605 305, <https://doi.org/10.1002/fld>, 2016.
- Mohammadi, B. and Pironneau, O.: *Applied Shape Optimization for fluids*, Oxford University Press, Oxford, 2nd editio edn., 2009.
- Okada, Y.: Internal deformation due to shear and tensile faults in a half-space, *Bulletin of the Seismological Society of America*, 82, 1018–  
1040, 1992.
- Palano, M., Puglisi, G., and Gresta, S.: Ground deformation patterns at Mt. Etna from 1993 to 2000 from joint use of InSAR and GPS  
610 techniques, *Journal of Volcanology and Geothermal Research*, 169, 99–120, <https://doi.org/10.1016/j.jvolgeores.2007.08.014>, 2008.
- Peltier, A., Staudacher, T., and Bachèlery, P.: Constraints on magma transfers and structures involved in the 2003 activity at Piton de La  
Founaise from displacement data, *Journal of Geophysical Research: Solid Earth*, 112, 1–16, <https://doi.org/10.1029/2006JB004379>, 2007.

- Peltier, A., Froger, J., Villeneuve, N., and Catry, T.: Assessing the reliability and consistency of InSAR and GNSS data for retrieving 3D-displacement rapid changes, the example of the 2015 Piton de la Fournaise eruptions, *Journal of Volcanology and Geothermal Research*, 344, 106–120, <https://doi.org/10.1016/j.jvolgeores.2017.03.027>, <http://dx.doi.org/10.1016/j.jvolgeores.2017.03.027>, 2017.
- 615 Raucoules, D., Maisons, C., Carnec, C., Le Mouelic, S., King, C., and Hosford, S.: Monitoring of slow ground deformation by ERS radar interferometry on the Vauvert salt mine (France): Comparison with ground-based measurement, *Remote Sensing of Environment*, 88, 468–478, <https://doi.org/10.1016/j.rse.2003.09.005>, 2003.
- Raucoules, D., Maisons, C., and Carnec, C.: Monitoring subsidence on the Vauvert salt mine using radar interferometry, in: *Journées Nationales de Géotechnique et de Géologie de l'ingénieur*, pp. 413–417, Lille, France, 2004.
- 620 Reilinger, R., McClusky, S., Vernant, P., Lawrence, S., Ergintav, S., Cakmak, R., Ozener, H., Kadirov, F., Guliev, I., Stepanyan, R., Nadariya, M., Hahubia, G., Mahmoud, S., Sakr, K., ArRajehi, A., Paradissis, D., Al-Aydrus, A., Prilepin, M., Guseva, T., Evren, E., Dmitrova, A., Filikov, S. V., Gomez, F., Al-Ghazzi, R., and Karam, G.: GPS constraints on continental deformation in the Africa-Arabia-Eurasia continental collision zone and implications for the dynamics of plate interactions, *Journal of Geophysical Research: Solid Earth*, 111, 1–26, <https://doi.org/10.1029/2005JB004051>, 2006.
- 625 Ritz, J.-F., Baize, S., Ferry, M., Larroque, C., Audin, L., Delouis, B., and Mathot, E.: The 11 November 2019 Mw 4.9 Le Teil earthquake surface rupture in France: new insight for seismic hazard in stable regions, *Communications Earth&Environnement - Nature*.
- Segall, P., Llenos, A. L., Yun, S.-H., Bradley, A. M., and Syracuse, E. M.: Time-dependent dike propagation from joint inversion of seismicity and deformation data, *Journal of Geophysical Research: Solid Earth*, 118, 5785–5804, <https://doi.org/10.1002/2013JB010251>, <http://doi.wiley.com/10.1002/2013JB010251>, 2013.
- 630 Smittarello, D., Cayol, V., Pinel, V., Froger, J. L., Peltier, A., and Dumont, Q.: Combining InSAR and GNSS to track magma transport at basaltic volcanoes, *Remote Sensing*, 11, 1–26, <https://doi.org/10.3390/rs11192236>, 2019.
- Valette, M.: Etude structurale du gisement salifère oligocène de Vauvert (Gard), Ph.D. thesis, Université de Montpellier, 1991.
- Valette, M. and Benedicto, A.: Gravity thrust halotectonics in the extensional Camargue basin (Gulf of Lion margin, SE France), *Bulletin de la Société Géologique de France*, 166, 137–147, 1995.
- 635 Van Sambek, L. L.: Evaluating Cavern Tests and Surface Subsidence Using Simple Numerical Models, *Seventh Symposium on salt*, 1, 433–439, 1993.
- Vasco, D. W., Ferretti, A., and Novali, F.: Reservoir monitoring and characterization using satellite geodetic data: Interferometric synthetic aperture radar observations from the Krechba field, Algeria, *Geophysics*, 73, WA113, <https://doi.org/10.1190/1.2981184>, 2008.
- 640 Wright, T. J., Parsons, B. E., and Lu, Z.: Toward mapping surface deformation in three dimensions using InSAR, *Geophysical Research Letters*, 31, 1–5, <https://doi.org/10.1029/2003GL018827>, 2004.
- Yamamoto, J. K.: Comparing ordinary kriging interpolation variance and indicator kriging conditional variance for assessing uncertainties at unsampled locations, in: *Application of Computers and Operations Research in the Mineral Industry - Proc. of the 32nd Int. Symposium on the Application of Computers and Operations Research in the Mineral Industry, APCOM 2005*, <https://doi.org/10.1201/9781439833407.ch34>, 2005.
- 645 Zhan, Y. and Gregg, P. M.: Data assimilation strategies for volcano geodesy, *Journal of Volcanology and Geothermal Research*, 2017.